

Non-linear vibrating Systems Excited by a Nonideal Energy Source with a Large Slope Characteristic

Javier González-Carbajal, Jaime Domínguez

Department of Mechanical and Manufacturing Engineering, University of Seville. C/ Camino de los Descubrimientos s/n, Isla de la Cartuja. 41092 Seville, Spain

e – mail: jgcarbajal@us.es, jaime@us.es

Abstract

This paper revisits the problem of an unbalanced motor attached to a fixed frame by means of a nonlinear spring and a linear damper. The excitation provided by the motor is, in general, nonideal, which means it is affected by the vibratory response. Since the system behaviour is highly dependent on the order of magnitude of the motor characteristic slope, the case of large slope is considered herein. Some Perturbation Methods are applied to the system of equations, which allows transforming the original 4D system into a much simpler 2D system. The fixed points of this reduced system and their stability are carefully studied. We find the existence of a Hopf bifurcation which, to the authors' knowledge, has not been addressed before in the literature. These analytical results are supported by numerical simulations. We also compare our approach and results with those published by other authors.

Keywords Nonideal Interaction · Unbalanced Motor · Singular Perturbation Theory · Averaging Method

1. Introduction

The motion of unbalanced rotors constitutes one of the most common vibration sources in mechanical engineering [1,2]. Vibrations due to unbalance may occur in any kind of rotating systems, such as turbines, flywheels, blowers or fans [3]. Actually, in practice, rotors can never be completely balanced because of manufacturing errors such as porosity in casting, non-uniform density of the material, manufacturing tolerances, etc. [4]. Even a subsequent balancing process will never be perfect due to the tolerances of the balancing machines.

Usually, rotor unbalance has a harmful effect on rotating machinery, since vibration may damage critical parts of the machine, such as bearings, seals, gears and couplings [4]. However, there are applications where

unbalanced rotors are used to generate a desired vibration. Some examples are the feeding, conveying and screening of bulk materials, or the vibrocompaction of quartz agglomerates, which makes use of unbalanced motors to compact a quartz-resin mixture. Actually, our interest in this vibrocompaction process has been the motivation for the presented study.

A simple model to analyse the dynamic response of a structure to the excitation produced by an unbalanced motor is sketched in **Fig. 2**. The simplest approach to this problem consists in assuming the rotor speed to be either constant or a prescribed function of time. In the constant speed case, the centrifugal force on the unbalance produces a harmonic excitation on the vibrating system, whose amplitude grows with the square of the rotating speed and whose frequency coincides with the rotating speed [3,5].

Note that, with this approach, it is implicitly being assumed that the rotational motion of the motor is independent of the vibration of the structure. This property is what defines an ideal excitation: it remains unaffected by the vibrating system response. Thus, the amplitude and frequency of an ideal excitation are known a priori, before solving the vibration problem. Obviously, this notion of ideality is applicable to any kind of excitation, and not only to the one produced by an unbalanced motor.

The ideality assumption is valid, with good approximation, in many real problems. However, there are situations where it is not. In 1904, Sommerfeld [6], whose pioneering work inspired many subsequent investigations, found experimentally kinds of behaviour which could not be explained upon the ideality hypothesis. He mounted an unbalanced electric motor on an elastically supported table and monitored the input power as well as the frequency and amplitude of the response [7]. The experiment consisted in increasing continuously the power input in order to make the rotor speed pass through the resonance frequency of the table, and then conduct the inverse process by decreasing the input power. The results obtained by Sommerfeld are qualitatively depicted in **Fig. 1**. When the rotor speed was close to resonance, an increment of the input power produced only a very slight increase of the rotor speed, while the oscillation amplitude increased considerably. This means that, in this part of the experiment, the increasing input power was not making the motor rotate faster, but was giving rise to larger oscillations. With further increasing of the input power, the rotor speed jumped abruptly to a frequency above resonance and, at the same time, the vibration amplitude jumped to a much smaller quantity than measured in the resonance region. When the process was reversed, by decreasing the motor input power, a jump phenomenon in the resonance region was also observed (see **Fig. 1**). However, this jump was found to be different to the one obtained for increasing rotor speed. This anomalous behaviour is usually referred to as ‘**The Sommerfeld Effect**’. An explanation for this phenomenon will be given in Section 4.1 of the present paper.

In 1969 [8], Kononenko published a book entirely devoted to the study of nonideal excitations. He considered different configurations of vibrating systems excited by nonideal motors and applied the Averaging Method to the equations of motion. By taking into account the two-way interaction between the motor and the vibrating structure, he was able to explain the nonlinear phenomena found by Sommerfeld. According to Kononenko, the Sommerfeld effect is produced by the torque on the rotor due to vibration of the unbalanced mass.

Rand et al. [9] reported the detrimental effect of a nonideal energy source in dual spin spacecrafts, which could endanger a particular manoeuvre of the spacecraft, once placed in orbit.

Although most studies use averaging procedures to obtain approximate solutions to the equations of motion, Blekhman [10] proposed an alternative approach, based on the method of ‘Direct Separation of Motions’.

Several authors, like El-Badawi [11] and Bolla et al. [12], analysed models where the vibrating system included an intrinsic cubic nonlinearity, in addition to the nonlinearity associated to the nonideal coupling between exciter and structure. Furthermore, Neimark-Sacker bifurcations were recently found in nonideal systems [13].

Balthazar et al. [14] published an extensive exposition of the state of the art concerning nonideal excitations.

A significant portion of the research effort on nonideal excitations has been directed to the analytical resolution of the equations of motion by means of perturbation techniques, especially the Averaging Method. A crucial point in these studies is the stability analysis of the stationary solutions near resonance. We find that, in some of these works, the assumptions made when applying perturbation methods can lead to inaccurate conclusions about stability. In view of this, a new analytical approach is proposed herein which includes the application of the Singular Perturbation Theory, besides the Averaging Method. Clearly, these procedures are classical in the analysis of nonlinear systems, but the combination of both in the study of nonideal excitations is actually a novel approach to the problem. This analytical scheme allows finding conditions for the existence of Hopf bifurcations, which have not been reported before, to the best of the authors’ knowledge.

The averaging methods constitute a very powerful tool which allows simplifying dynamical systems where one or more variables exhibit a small, fast oscillation superimposed on a slow variation of its mean value. The analytical procedure lies on neglecting the fast oscillations and looking for an asymptotic approximation to the slowly evolving average. The interested reader can refer to [15].

The Singular Perturbation Theory deals with dynamical systems where some state variables are fast and some are slow. Under certain conditions, the behaviour of the system in the phase space can be shown to be composed of two subsequent stages. During the first one, trajectories are rapidly attracted towards a particular surface, known as the Slow Manifold. In the second stage, the system slowly evolves along the Slow Manifold, with the fast variables being slaved to the slow ones. This peculiar behaviour allows the system dimension to be reduced during the second stage, for the fast variables can be expressed as functions of the slow ones. For a detailed treatment, see [16–18].

Hopf bifurcations constitute a common mechanism whereby a fixed point of a dynamical system loses stability. As it is well known, the stability of an equilibrium point is given by the real parts of the eigenvalues of the system jacobian matrix. A Hopf bifurcation occurs –with the exception of some degenerate cases– when two complex conjugate eigenvalues cross the imaginary axis. A very interesting feature of Hopf bifurcations is the appearance of limit cycles surrounding the bifurcating equilibrium point. Extensive analysis of this matter can be found in [19,20].

Finally, it is convenient to position the present work within the literature, showing its similarities and differences with respect to previous publications.

First, it should be noted that the Hopf bifurcation found in this paper is conceptually different to that reported in [21]. The reason is that, while we investigate here the fixed points of an averaged system, representing stationary motions of the motor, Dantas et al. analyzed in [21] the fixed points of the original system of equations, corresponding to the motor at rest.

It should also be stressed that the present article is mainly based on analytical results, which are validated by numerical simulations. This makes it substantially different to several other works where conclusions are directly drawn from numerical experiments [22–24].

The mechanical system analyzed in this paper is very similar to that studied by Fidlin in [25] and Sanders et al. in [15]. However, they considered the slope of the motor characteristic to be a small parameter, while our assumption is the opposite. In fact, the motor characteristic slope is a chief parameter of the problem. The system exhibits different behaviors and requires different mathematical approaches depending on the order of magnitude of this parameter.

The mechanical system that we investigate is also akin to that studied by Rand et al. in [9,26]. However, they considered an undamped vibrating system and a motor driven by a constant torque. Due to these differences the analytical approach and the conclusions of this paper are significantly different to those reported in [9,26].

There are also published works where chaotic motions are found in systems excited by nonideal power sources [24,27,28]. However, as long as the assumptions specified in Section 2 hold, this kind of behavior is not possible for the particular system under study. The reason is that, as shown in Section 2, the reduced system has only 2 dimensions, while at least 3 dimensions are needed to find chaos.

The paper is organized as follows. Section 2 poses the equations of motion of the system under study and specifies the assumptions on which our analysis is based. In Section 3, we make use of some perturbation techniques to transform the original 4D system into a simpler 2D reduced system. In Section 4, the fixed points of this reduced system are obtained and their stability is assessed. Under some conditions, we prove the existence of a Hopf bifurcation, which makes the unstable region larger than predicted by other theories. Thus, not taking it into account might be dangerous for real applications, since the system could exhibit unexpected instabilities. Section 5 presents the results of some numerical experiments in order to validate the analytical developments of Sections 3 and 4. Section 6 is intended to discuss our results and compare them with those of other authors. Finally, Section 7 summarises the main conclusions of our study.

2. Problem statement and assumptions

Consider the system depicted in **Fig. 2**. It consists of an unbalanced motor attached to a fixed frame by a nonlinear spring –whose force has linear and cubic components– and a linear damper. The cubic component of the spring gives the possibility to model a nonlinear behavior for the structure supporting the motor [29].

The effect of gravity can be shown to have no relevance [30], so it will not be included in the model.

Variable x stands for the linear motion, ϕ is the angle of the rotor, m_1 is the unbalanced mass with eccentricity r , m_0 is the rest of the vibrating mass, I_0 is the rotor inertia (without including the unbalance), b is the damping coefficient and k and λ are, respectively, the linear and cubic coefficients of the spring. The equations of motion for the coupled 2– DOF system are [11]

$$\begin{aligned} m\ddot{x} + b\dot{x} + kx + \lambda x^3 &= m_1 r (\dot{\phi}^2 \cos \phi + \ddot{\phi} \sin \phi) \\ I\ddot{\phi} &= L(\dot{\phi}) + m_1 r \ddot{x} \sin \phi, \end{aligned} \quad (1)$$

where $m = m_0 + m_1$, $I = I_0 + m_1 r^2$. A dot represents differentiation with respect to time, t .

Function $L(\dot{\phi})$ is the driving torque produced by the motor –given by its static characteristic– minus the losses torque due to friction at the bearings, windage, etc. We assume this net torque to be a linear function of the rotor speed

$$L(\dot{\phi}) = C + D(\dot{\phi} - \omega_n), \quad (2)$$

where ω_n is the linear natural frequency of the oscillator, given by $\omega_n = \sqrt{k/m}$. More complex curves for the driving torque have been studied in [31]. Although $L(\dot{\phi})$ includes the damping of rotational motion, we will usually refer to it shortly as ‘**the motor characteristic**’. We further assume $D < 0$ –the driving torque decreases with the rotor speed–, as is usual for most kinds of motor. This assumption will prove to be of major importance.

By defining

$$\begin{aligned} R_m &= m_1/m, \quad R_I = m_1 r^2/I \\ \xi &= \frac{b}{2\sqrt{km}}, \quad \alpha = \frac{R_I R_m}{2\xi} \\ c &= \frac{C}{I\omega_n^2}, \quad d = \frac{D}{I\omega_n}, \quad \tau = \omega_n t \\ u &= \frac{x}{r} \frac{2\xi}{R_m}, \quad \rho = \frac{\lambda r^2}{k} \left(\frac{R_m}{2\xi} \right)^2, \end{aligned} \quad (3)$$

the equations of motion can be written in a more convenient dimensionless form

$$\begin{aligned} \ddot{u} + u &= -2\xi\dot{u} - \rho u^3 + 2\xi(\dot{\phi}^2 \cos \phi + \ddot{\phi} \sin \phi) \\ \ddot{\phi} &= c + d(\dot{\phi} - 1) + \alpha\dot{u} \sin \phi, \end{aligned} \quad (4)$$

where a dot now represents differentiation with respect to dimensionless time, τ .

In order to apply perturbation techniques to system (4), some assumptions on the order of magnitude of the system parameters have to be made. Thus, the damping, the unbalance and the nonlinearity are assumed to be

small. This is expressed by making the corresponding coefficients proportional to a sufficiently small, positive and dimensionless parameter ϵ :

$$\xi = \epsilon\xi_0, \quad \alpha = \epsilon\alpha_0, \quad \rho = \epsilon\rho_0. \quad (5)$$

The torque generated by the motor at resonance ($\dot{\phi} = 1$) is also assumed to be sufficiently small:

$$c = \epsilon c_0. \quad (6)$$

Finally, the slope of the motor characteristic is assumed to be of the order of unity, i.e. independent of ϵ :

$$d = d_0. \quad (7)$$

This assumption corresponds to what we have called *large slope characteristic*. The case of small slope, with d proportional to ϵ , is treated in [25]. It is worth noting that the case of *small slope characteristic* requires a different mathematical approach and displays substantially different dynamics.

Taking the proposed scaling (5-7) into account and dropping the subscript ‘0’ for convenience, (4) can be written as

$$\begin{aligned} \ddot{u} + u &= \epsilon\{-2\xi\dot{u} - \rho u^3 + 2\xi(\dot{\phi}^2 \cos \phi + \ddot{\phi} \sin \phi)\} \\ \ddot{\phi} &= d(\dot{\phi} - 1) + \epsilon\{c + \alpha\ddot{u} \sin \phi\}. \end{aligned} \quad (8)$$

3. Perturbation Approach: Derivation of the Reduced System

Equations (8) constitute an autonomous dynamical system of dimension 4, with state variables $\{u, \dot{u}, \phi, \dot{\phi}\}$. In this Section we propose a perturbation approach intended to transform (8) into an approximate 2D system, much easier to analyze.

First, it is convenient to perform a change of variables, from $\{u, \dot{u}\}$ to polar coordinates:

$$\begin{aligned} u &= a \cos(\phi + \beta) \\ \dot{u} &= -a \sin(\phi + \beta). \end{aligned} \quad (9)$$

This step does not include any approximation, since we are just replacing the pair of variables $\{u(\tau), \dot{u}(\tau)\}$ with the pair of amplitude–phase variables $\{a(\tau), \beta(\tau)\}$.

By differentiating the first of relations (9) we obtain

$$\dot{u} = \dot{a} \cos(\phi + \beta) - a(\dot{\phi} + \dot{\beta}) \sin(\phi + \beta). \quad (10)$$

Comparing (10) with the second of relations (9) yields

$$\dot{a} \cos(\phi + \beta) - a(\dot{\phi} - 1 + \dot{\beta}) \sin(\phi + \beta) = 0. \quad (11)$$

On the other hand, if we introduce (9) into the first of equations (8), we have

$$\begin{aligned} & -\dot{a} \sin(\phi + \beta) - a(\dot{\phi} - 1 + \dot{\beta}) \cos(\phi + \beta) = \\ & = \epsilon \{ 2\xi a \sin(\phi + \beta) - \rho a^3 \cos^3(\phi + \beta) + 2\xi(\dot{\phi}^2 \cos \phi + \ddot{\phi} \sin \phi) \}. \end{aligned} \quad (12)$$

Equations (11) and (12) together form a linear system for \dot{a} and $\dot{\beta}$ that can be readily solved:

$$\left\{ \begin{array}{l} \dot{a} = -\epsilon \sin(\phi + \beta) \{ 2\xi a \sin(\phi + \beta) - \rho a^3 \cos^3(\phi + \beta) + 2\xi(\dot{\phi}^2 \cos \phi + \ddot{\phi} \sin \phi) \} \\ \dot{\beta} = 1 - \dot{\phi} - \epsilon \frac{\cos(\phi + \beta)}{a} \{ 2\xi a \sin(\phi + \beta) - \rho a^3 \cos^3(\phi + \beta) + 2\xi(\dot{\phi}^2 \cos \phi + \ddot{\phi} \sin \phi) \} \end{array} \right\}. \quad (13)$$

It is also suitable to define a new variable for the rotor speed:

$$\Omega \equiv \dot{\phi}. \quad (14)$$

Then, the dynamical system, written in terms of the new variables, becomes

$$\left\{ \begin{array}{l} \dot{a} = -\epsilon \sin(\phi + \beta) F_1(a, \beta, \phi, \Omega) + O(\epsilon^2) \\ \dot{\beta} = 1 - \Omega - \epsilon \frac{\cos(\phi + \beta)}{a} F_1(a, \beta, \phi, \Omega) + O(\epsilon^2) \\ \dot{\Omega} = \left\{ \begin{array}{l} d(\Omega - 1) + \\ + \epsilon(c - \alpha a \sin \phi \cos(\phi + \beta)) \end{array} \right\} + O(\epsilon^2) \\ \dot{\phi} = \Omega \end{array} \right\}, \quad (15)$$

where

$$F_1 = \left\{ \begin{array}{l} 2\xi a \sin(\phi + \beta) - \rho a^3 \cos^3(\phi + \beta) + \\ + 2\xi[\Omega^2 \cos \phi + d(\Omega - 1) \sin \phi] \end{array} \right\}. \quad (16)$$

We have derived a new 4D autonomous dynamical system (15), with state variables $\{a, \beta, \phi, \Omega\}$, which is fully equivalent to (8).

Consider now a general set of initial conditions $\{a_0, \beta_0, \phi_0, \Omega_0\}$ and let us investigate how the variables evolve with time. In the next subsections, it will be shown that the dynamics of (15) is composed of three consecutive stages of time, with different qualitative behaviors.

3.1. First stage

Let us only consider, for the moment, the evolution equations for variables β and Ω . They can be written as

$$\begin{aligned}\dot{\beta} &= 1 - \Omega + O(\epsilon) \\ \dot{\Omega} &= d(\Omega - 1) + O(\epsilon).\end{aligned}\tag{17}$$

Then, it is clear that, to first order of approximation, the evolution of β and Ω only depends on Ω . This first order approximation corresponds to neglecting the $O(\epsilon)$ terms in (17):

$$\begin{aligned}\dot{\beta} &= 1 - \Omega \\ \dot{\Omega} &= d(\Omega - 1).\end{aligned}\tag{18}$$

The relation between exact system (17) and approximate system (18) is established by the Regular Perturbation Theory [15], which assures that solutions of (18) are $O(\epsilon)$ -approximations to solutions of (17), for $\tau = O(1)$. Thus, we proceed to solve system (18):

$$\begin{aligned}\beta &= \beta_0^* + \frac{1 - \Omega_0}{d} e^{d\tau} \\ \Omega &= 1 + [\Omega_0 - 1]e^{d\tau},\end{aligned}\tag{19}$$

with

$$\beta_0^* \equiv \beta_0 + \frac{\Omega_0 - 1}{d}.\tag{20}$$

It is clear from (19) that both variables tend exponentially to constant values:

$$\beta \rightarrow \beta_0^*, \quad \Omega \rightarrow 1.\tag{21}$$

This is due to the assumption $d < 0$, since, otherwise, the exponentials in (19) would be divergent. Taking into account the approximation made when transforming (17) into (18), we can state that, after a time interval $\tau = O(1)$, we have

$$\beta = \beta_0^* + O(\epsilon), \quad \Omega = 1 + O(\epsilon).\tag{22}$$

Once β and Ω are at an $O(\epsilon)$ -distance from β_0^* and 1, respectively, the first stage of the motion is over. Note that, during this stage, the rotor speed evolves monotonically towards the resonance region.

Throughout the first phase, variable a remains nearly constant. Since $\dot{a} = O(\epsilon)$ –see (15)–, variable a needs a time length $\tau = O(1/\epsilon)$ to evolve significantly. Thus, at the end of the first stage, we have

$$a = a_0 + O(\epsilon).\tag{23}$$

In summary, the first stage corresponds to a time length $\tau = O(1)$. It starts at $\tau = 0$ and it ends when β and Ω have reached an $O(\epsilon)$ -distance to β_0^* and 1, respectively.

3.2. Second stage

At the beginning of the second stage, the rotor speed is already in the vicinity of resonance, so let us expand it as

$$\Omega = 1 + \epsilon\sigma. \quad (24)$$

If system (15) is written using variable σ instead of Ω , we have

$$\begin{aligned} \dot{a} &= -\epsilon \sin(\phi + \beta) F_2(a, \beta, \phi) + O(\epsilon^2) \\ \dot{\beta} &= -\epsilon\sigma - \epsilon \frac{\cos(\phi + \beta)}{a} F_2(a, \beta, \phi) + O(\epsilon^2) \\ \dot{\sigma} &= c + d\sigma - \alpha a \sin \phi \cos(\phi + \beta) + O(\epsilon) \\ \dot{\phi} &= 1 + \epsilon\sigma, \end{aligned} \quad (25)$$

where

$$F_2 = \left\{ \begin{aligned} &2\xi a \sin(\phi + \beta) - \rho a^3 \cos^3(\phi + \beta) + \\ &+ 2\xi \cos \phi \end{aligned} \right\}. \quad (26)$$

Notice that the closeness between the rotor speed and the natural frequency of the system has transformed β into a slow variable.

With the aim of analyzing the second and third stages of the motion, the Averaging Method is applied to system (25).

First, let us define the averaged variables as

$$\bar{a}(\tau) \equiv \frac{1}{2\pi} \int_{\tau-\pi}^{\tau+\pi} a(s) ds, \quad (27)$$

with analogous definitions for $\bar{\beta}$ and $\bar{\sigma}$.

Now, let us focus on the evolution of the averaged variables. The equations that govern their dynamics can be obtained by averaging system (25), i.e. applying to system (25) the operator defined in (27). After some manipulations, which are detailed in the Appendix, we arrive at the averaged system

$$\begin{aligned} \dot{a} &= -\epsilon\xi(a + \sin \beta) + O(\epsilon^2) \\ \dot{\beta} &= -\epsilon \left(\sigma + \xi \frac{\cos \beta}{a} - \frac{3}{8} \rho a^2 \right) + O(\epsilon^2) \\ \dot{\sigma} &= c + d\sigma + \frac{\alpha}{2} a \sin \beta + O(\epsilon), \end{aligned} \quad (28)$$

where the overbars have been omitted for simplicity.

It is convenient to highlight the relation between the original and the averaged variables. In order to do so, observe from (25) that a and β are slow variables, while σ is a fast variable. This implies that, in one averaging period of length 2π , variables a and β can only move an $O(\epsilon)$ -distance away from their averages. Conversely, σ is able to move an $O(1)$ -distance away from $\bar{\sigma}$. This can be written as

$$\begin{aligned} a &= \bar{a} + O(\epsilon) \\ \beta &= \bar{\beta} + O(\epsilon) \\ \sigma &= \bar{\sigma} + O(1). \end{aligned} \quad (29)$$

Observe that, even with an $O(1)$ error in σ , we still know the rotor speed with $O(\epsilon)$ precision, since $\Omega = 1 + O(\epsilon)$. From now on, the overbars will be omitted, unless otherwise stated.

The task now is to investigate system (28). As pointed out before, this is a fast-slow system, with two slow variables a and β and one fast variable σ . This difference in the time scales allows exploiting the Singular Perturbation Theory (SPT) [16–18].

According to the SPT, a system with the form of (28) displays two qualitatively different behaviors at two sequential time scales, which correspond to the second and third stages of the original system (15). With the aim of studying the first of them –second stage of (15)–, consider a time interval $\tau = O(1)$ for system (28). Since a and β evolve with rate $O(\epsilon)$, it is clear that we have

$$\begin{aligned} a &= a_0 + O(\epsilon) \\ \beta &= \beta_0^* + O(\epsilon) \\ \dot{\sigma} &= c + d\sigma + \frac{\alpha}{2} a_0 \sin \beta_0^* + O(\epsilon), \end{aligned} \quad (30)$$

where we have taken into account that, at the beginning of stage 2, $a = a_0 + O(\epsilon)$ and $\beta = \beta_0^* + O(\epsilon)$.

Then, the only variable that changes considerably during this stage is σ . From a direct analysis of the last of equations (30), it can be deduced that σ tends exponentially to the following value

$$\sigma \rightarrow -\frac{c}{d} - \frac{\alpha}{2d} a_0 \sin \beta_0^*, \quad (31)$$

which is the only fixed point for the last of equations (30). The assumption $d < 0$ guarantees that the fixed point is globally attracting.

Expression (31), generalized to any values of a and β , gives what is called ‘the Slow Manifold’:

$$\sigma^*(a, \beta) = -\frac{c}{d} - \frac{\alpha}{2d} a \sin \beta. \quad (32)$$

Thus, (31) can be rewritten as

$$\sigma \rightarrow \sigma^*(a_0, \beta_0^*). \quad (33)$$

Thereby, at this stage, the slow variables remain almost constant, while the fast variable evolves until reaching the vicinity of the slow manifold.

Summing up, the second stage corresponds to a time length $\tau = O(1)$, just as the first one. It ends once variable σ has reached an $O(\epsilon)$ -distance to $\sigma^*(a_0, \beta_0^*)$. During this phase of the motion, a and β do not change significantly.

3.3. Third stage

The third stage of the original system (15) –which is the second stage of the averaged system (28)– occurs at a time scale $\tau = O(1/\epsilon)$. This can be easily understood by noticing that, once the system is near the slow manifold, variable σ becomes slow (introducing (32) in (28) leads to $\dot{\sigma} = O(\epsilon)$). Therefore, near the slow manifold, all variables are slow and, as a consequence, the system natural time scale is $\tau = O(1/\epsilon)$.

As a relevant step in the application of the SPT, the attractiveness of the slow manifold has to be guaranteed. Then, consider the fast subsystem, given by

$$\dot{\sigma} = c + d\sigma + \frac{\alpha}{2} a \sin \beta, \quad (34)$$

with a and β fixed. Clearly, for any possible values of a and β , subsystem (34) is always attracted towards fixed point

$$\sigma = \sigma^*(a, \beta) = -\frac{c}{d} - \frac{\alpha}{2d} a \sin \beta, \quad (35)$$

by virtue of the assumption $d < 0$. Then, the slow manifold is attractive and, therefore, once the system is near the slow manifold, it remains in its neighborhood for all subsequent time [17,18,32].

By introducing the expression of the slow manifold in (28), the equations corresponding to the third phase of the motion are obtained:

$$\begin{aligned} \dot{a} &= -\epsilon \xi (a + \sin \beta) + O(\epsilon^2) \\ \dot{\beta} &= -\epsilon \left(\sigma^*(a, \beta) + \xi \frac{\cos \beta}{a} - \frac{3}{8} \rho a^2 \right) + O(\epsilon^2) \\ \sigma &= \sigma^*(a, \beta) + O(\epsilon). \end{aligned} \quad (36)$$

As usual, we can eliminate higher order terms in (36), giving rise to an $O(\epsilon)$ approximation for a time length $\tau = O(1/\epsilon)$:

$$\begin{aligned} \dot{a} &= -\epsilon \xi (a + \sin \beta) \\ \dot{\beta} &= -\epsilon \left(\sigma^*(a, \beta) + \xi \frac{\cos \beta}{a} - \frac{3}{8} \rho a^2 \right) \\ \sigma &= \sigma^*(a, \beta). \end{aligned} \quad (37)$$

It is convenient to observe that, although (37) contains three equations, only two of them are differential equations. Thus, (37) represents a 2D autonomous dynamical system. The evolution of a and β no longer depends on σ , once σ is written as a function of a and β . The last equation is written with the only purpose of tracking the evolution of variable σ .

In summary, the third stage corresponds to a time length $\tau = O(1/\epsilon)$. At this phase of the motion, the averaged system evolves along the slow manifold given by (32). Variables a , β and σ obey equations (37), with $O(\epsilon)$ precision.

Fig. 2 shows a schematic representation of the the three different stages of the system dynamics, summing up the results obtained in the present Section. Note that, in **Fig. 2**, we recover the use of overbars for the averaged variables. The most relevant result is that, once the initial transient corresponding to the first two stages has finished, the evolution of variables a and β is governed by equations (37) –within an $O(\epsilon)$ error–.

From **Fig. 2**, it is clear that suitable initial conditions for system (37) are $\{a_0, \beta_0^*\}$. Recalling definition (20), this can be written as $\{a_0, \beta_0 + (\Omega_0 - 1)/d\}$, where $\{a_0, \beta_0, \phi_0, \Omega_0\}$ is the set of initial conditions for system (15).

However, we may be interested in a particular set of initial conditions for system (8), given as $\{u_0, \dot{u}_0, \phi_0, \dot{\phi}_0\}$. It is, then, convenient, to express the initial conditions for (37) as functions of the initial conditions for (8):

$$\begin{aligned} a_0 &= \sqrt{u_0^2 + \dot{u}_0^2} \\ \beta_0^* &= \tan^{-1}\left(\frac{-\dot{u}_0}{u_0}\right) - \phi_0 + \frac{\dot{\phi}_0 - 1}{d}, \end{aligned} \quad (38)$$

as can be readily deduced from relations (9),(14) and (20).

Recapitulating, we have been able to eliminate variable ϕ from the formulation by Averaging, and variable σ by applying the Singular Perturbation Theory. It is also worth noting that, although some authors have found chaotic motions in nonideal systems [24,27], this kind of behavior is not possible for the particular case under study. The reason is that at least 3 dimensions are needed to have chaos, while our reduced system (37) is of dimension 2.

4. Analysis of the Reduced System

This Section focuses on the behaviour of system (37), once its solutions have been shown to be good approximations to those of the original system.

Firstly, it is useful to make a comparison between the system under study and its ideal counterpart, where the rotor speed is constant. Clearly, for this ideal case, the equation of motion of the system shown in **Fig. 2** is given by

$$m\ddot{x} + b\dot{x} + kx + \lambda x^3 = m_1 r \dot{\phi}^2 \cos \phi, \quad (39)$$

with $\dot{\phi}$ fixed. Equation (39) describes a Duffing oscillator, subjected to harmonic excitation. This is a very well-known problem, which has been widely studied in the literature [7,25,33–35]. Under the assumptions of small damping, small nonlinearity, small unbalance and near-resonant excitation ($\dot{\phi} = 1 + \epsilon\sigma_0$), the Averaging Method can be applied to system (39), leading to

$$\begin{aligned} \dot{a} &= -\epsilon\xi(a + \sin \beta) \\ \dot{\beta} &= -\epsilon\left(\sigma_0 + \xi \frac{\cos \beta}{a} - \frac{3}{8}\rho a^2\right), \end{aligned} \quad (40)$$

where all the parameters and variables are defined as in Sections 2 and 3. It is easy to verify that system (40) is exactly the same as (37), with the only difference of replacing $\sigma^*(a, \beta)$ by the constant value σ_0 . This is a clear illustration of the concept of nonideal excitation. In the ideal case, the rotor speed appears in equations (40) as a constant value σ_0 , externally imposed by the motor. However, in the nonideal case, the rotor speed enters equations (37) as a function of the system vibratory motion, $\sigma^*(a, \beta)$.

It is also important to observe that an ideal motor displays a vertical static characteristic, corresponding to the limit case $d \rightarrow -\infty$. The motor is, then, able to generate any torque for the same rotor speed. This suggests the idea that a real motor with a static characteristic of very large slope (in absolute value) is more likely to behave in an ideal manner than another one with a smaller slope.

4.1. Fixed Points

Going back to the objective of analyzing system (37), let us first look for its fixed points, $\{a_{eq}, \beta_{eq}, \sigma_{eq}\}$:

$$\begin{aligned} a_{eq} &= -\sin \beta_{eq} \\ \sigma^*(a_{eq}, \beta_{eq}) &= \frac{3}{8}\rho a_{eq}^2 - \xi \frac{\cos \beta_{eq}}{a_{eq}} \\ \sigma_{eq} &= \sigma^*(a_{eq}, \beta_{eq}). \end{aligned} \quad (41)$$

From the first of equations (41), we have

$$\cos \beta_{eq} = -z \sqrt{1 - a_{eq}^2}, \quad z = \pm 1. \quad (42)$$

Combining (32), (41) and (42), we arrive at

$$-\frac{c}{d} + \frac{\alpha}{2d} a_{eq}^2 = \frac{3}{8}\rho a_{eq}^2 + z\xi \frac{\sqrt{1 - a_{eq}^2}}{a_{eq}}. \quad (43)$$

Solutions of (43), for both values of z , give a_{eq} for all the fixed points of (37). However, it is not straightforward to solve (43), for a_{eq} , analytically. We propose an alternative procedure, which leads to the fixed points of (37) in a graphical way. In order to do so, let us rewrite the last of equations (37) as

$$c + d\sigma = -\frac{\alpha}{2}a \sin \beta, \quad (44)$$

where the definition (32) of $\sigma^*(a, \beta)$ has been used. Now, recall the last of equations (28), which governs the evolution of the rotor speed for the averaged system:

$$\dot{\sigma} = c + d\sigma + \frac{\alpha}{2}a \sin \beta + O(\epsilon). \quad (45)$$

In the light of (45) we can interpret (44) as an equilibrium between two torques on the rotor. The left hand term in (44) represents the driving torque produced by the motor, while the right hand term represents the resisting torque due to vibration. Thus, the fact that the averaged system is on the slow manifold –which is expressed in equation (44)– can be understood as a torque equilibrium condition.

Equation (44), particularized for the fixed point $\{a_{eq}, \beta_{eq}, \sigma_{eq}\}$ takes the form

$$c + d\sigma_{eq} = \frac{\alpha}{2}a_{eq}^2, \quad (46)$$

where (41) has been used. We now define the following functions:

$$\begin{aligned} T_m(\sigma) &\equiv c + d\sigma \\ T_v(a) &\equiv \frac{\alpha}{2}a^2. \end{aligned} \quad (47)$$

Clearly, according to the comments below equation (45), T_m represents the driving torque produced by the motor, while T_v corresponds to the resisting torque due to vibration. Then, equation (46) can be written as

$$T_m(\sigma_{eq}) = T_v(a_{eq}), \quad (48)$$

which is the torque equilibrium condition, particularized for the fixed point.

In order to solve (48) in a graphical way, we would like to write both torques explicitly in terms of σ_{eq} . However, this would in turn need explicitly writing a_{eq} in terms of σ_{eq} , which is not straightforward. Thus, we resort to an implicit procedure for the graphical representation. Combining (41) and (42), we have

$$\sigma_{eq} = \sigma_v(z, a_{eq}), \quad (49)$$

where function $\sigma_v(z, a)$ is defined as

$$\sigma_v(z, a) \equiv \frac{3}{8}\rho a^2 + z\xi \frac{\sqrt{1-a^2}}{a}. \quad (50)$$

The proposed representation can be constructed as follows: first, graph, T_m versus σ according to (47). Then, graph on the same plot the parametric curve given by $\{\sigma_v(z, a), T_v(a)\}$, for $z = \pm 1$ and $a \in (0,1]$. The fact that a is strictly positive comes from the definition of a as the radius of a polar coordinate transformation –see (9)–. On the other hand a_{eq} cannot be greater than 1, according to the first of equations (41).

The above procedure gives rise to a plot like that shown in **Fig. 4**. Considering equation (48), we can find the fixed points as the intersections of the two torque curves. In the particular case displayed in **Fig. 4**, there are three equilibrium points, marked with circles. Note that the curve associated to the vibration torque is composed of two branches, which collide at the maximum of the curve. They correspond to the two possible values of parameter z , as specified in **Fig. 4**.

We note that the ‘Sommerfed effect’, which was described in the introduction and depicted in **Fig. 1**, can be readily explained by using the torque-speed curves. This explanation is graphically shown in **Fig. 5**. Suppose that the motor is controlled by displacing its characteristic parallel to itself. This is actually the case, for instance, in simplest control approach for an induction motor, known as the V/f control [36]. Then, for increasing (decreasing) input power, the motor curve is displaced upwards (downwards). Consider the first part of Sommerfeld’s experiment, where the input power is increased so as to make the rotor speed pass through the system natural frequency. As depicted in **Fig. 5**, when the system approaches resonance, the increase in the rotor speed is slowed down due to the presence of the resonance peak. This occurs until the motor curve becomes tangent to the vibration torque curve. At this point, the large-amplitude stationary motion disappears through a saddle-node bifurcation, as discussed by Kononenko [8], Dimentberg [30] and others [10,11,14].

The referred bifurcation makes the system jump towards the only remaining stationary motion, which is a post-resonant state with smaller vibration amplitude. A similar phenomenon takes place for decreasing frequency, although the jump is smaller in this case (see **Fig. 5**). This classical explanation is in accordance with the analyses given in [8,11,12,30].

Note that, in the above discussion, it is assumed that every fixed point between A and B , and between C and D , is stable. If the fixed point lost its stability before the tangency point B or D , then the jump phenomenon would occur before than predicted in **Fig. 5**. A detailed stability analysis of the fixed points is presented below.

4.2. Stability Analysis

Once the fixed points of the reduced system have been obtained, we turn to the analysis of their stability. For a 2D system, this reduces to calculating the trace and determinant of the jacobian matrix, evaluated at the equilibrium point of interest. In order to obtain this jacobian, consider the reduced system (37), which can be written as

$$\left\{ \begin{array}{l} \dot{a} = -\epsilon\xi(a + \sin\beta) \\ \dot{\beta} = \epsilon \left(\frac{c}{d} + \frac{\alpha}{2d}a \sin\beta - \xi \frac{\cos\beta}{a} + \frac{3}{8}\rho a^2 \right) \end{array} \right\}, \quad (51)$$

Note that the only difference between (37) and (51) is that expression (35) for $\sigma^*(a, \beta)$ has been introduced. The jacobian matrix of system (51), at the equilibrium point of interest, is obtained by partially differentiating each equation with respect to a and β , and particularizing for $\{a_{eq}, \beta_{eq}\}$. Making use of expressions (41) and (42), the obtained matrix is

$$J_{eq} = \epsilon \begin{bmatrix} -\xi & z\xi R_{eq} \\ \left(-\frac{\alpha}{2d} + \frac{3\rho}{4}\right)a_{eq} - \frac{z\xi R_{eq}}{a_{eq}^2} & -\frac{z\alpha a_{eq} R_{eq}}{2d} - \xi \end{bmatrix}, \quad (52)$$

where R_{eq} stands for $\sqrt{1 - a_{eq}^2}$. The conditions for a fixed point to be asymptotically stable are

$$\mathbf{C1.} \quad \text{tr}(J_{eq}) < 0 \quad (53)$$

$$\mathbf{C2.} \quad \det(J_{eq}) > 0. \quad (54)$$

After some algebra, these conditions can be expressed as

$$\mathbf{C1.} \quad \frac{z\alpha a_{eq} R_{eq}}{4d} + \xi > 0 \quad (55)$$

$$\mathbf{C2.} \quad \left\{ \begin{array}{ll} \frac{1}{\eta} - \frac{1}{d} < 0, & \text{if } z = 1 \\ \frac{1}{\eta} - \frac{1}{d} > 0, & \text{if } z = -1 \end{array} \right\}, \quad (56)$$

where η denotes the slope of the T_v curve at the considered equilibrium point, and has expression

$$\frac{1}{\eta} = -\frac{z\xi}{\alpha a_{eq}^3 R_{eq}} + \frac{3\rho}{4\alpha}, \quad (57)$$

as can be deduced from (47), (50).

We now apply conditions (55) and (56) to evaluate stability regions in different scenarios. The procedure is as follows. Consider parameters α, ξ, ρ fixed, so that the T_v curve –see **Fig. 4**– is fixed too. Consider a pair of values (c, d) which gives a particular curve $T_m(\sigma)$. The intersections between the two curves represent the equilibrium points of the system. Select one of them –if there are more than one– and let parameters (c, d) vary in such a way that the selected equilibrium point remains an equilibrium point. In other words, let parameters (c, d) vary so as to make the curve $T_m(\sigma)$ rotate around the selected equilibrium point, satisfying restriction $d < 0$. Finally, use conditions (55) and (56) to analyze how the stability of the fixed point is affected by the slope d of the motor characteristic.

Fig. 6 displays the outcome of applying the above procedure for a fixed point located at the left branch of the vibration torque curve ($z = -1$). Two scenarios are considered, depending on the sign of slope η , evaluated at the fixed point under consideration. It is observed that a change of stability occurs when both torque curves become tangent ($d = \eta$). This can be shown to correspond to a transcritical bifurcation.

Fig. 7 shows analogous results for a fixed point located at the right branch of the vibration torque curve ($z = 1$). The system behavior is richer in this case, since stability may change in two different ways, depending on the comparison $\eta \lesseqgtr d_H$.

We define critical slope d_H as the value of d which makes $\text{tr}(J_{eq}) = 0$. Recall that the stability condition $\text{tr}(J_{eq}) < 0$ was written as (55). Therefore, d_H takes the form

$$d_H(\alpha, \xi, a_{eq}) = -\frac{\alpha a_{eq} R_{eq}}{4\xi}. \quad (58)$$

Let us consider the different possibilities for $z = 1$.

If $\eta > 0$ (**Fig. 7a**), condition **C2** is never fulfilled, so the fixed point is unstable regardless the value of slope d .

If $\eta < d_H < 0$ (**Fig. 7b.1**), the critical condition –i.e. the one which produces the stability change– is **C2**. In this case, a transcritical bifurcation can be shown to occur when both torque curves are tangent ($d = \eta$). Note that this result is analogous to that obtained for the left branch (**Fig. 6**).

If $d_H < \eta < 0$ (**Fig. 7b.2**), the critical condition is **C1**. In this case, the stability change occurs at $d = d_H$ through a Hopf bifurcation, after which we named parameter d_H .

To better understand the nature of the different bifurcations, notice the following correspondence between conditions **C1** and **C2**, and the eigenvalues of J_{eq} , according to (53), (54):

- **C1** is the critical condition $\rightarrow \left\{ \begin{array}{l} \text{tr}(J_{eq}) = 0 \\ \det(J_{eq}) > 0 \end{array} \right\}$ both eigenvalues of J_{eq} , being complex conjugates, cross the imaginary axis.
- **C2** is the critical condition $\rightarrow \left\{ \begin{array}{l} \text{tr}(J_{eq}) < 0 \\ \det(J_{eq}) = 0 \end{array} \right\}$ a single, real eigenvalue of J_{eq} crosses the imaginary axis.

It should be stressed that most of the literature on nonideal excitations maintains that stability changes when the torque curves become tangent [7,8,10,30]. This is consistent with the results of the present paper, with the important exception of case $z = 1, d_H < \eta < 0$ (**Fig. 7b.2**). Thus, one of the main contributions of this paper consists in having found a case where the usual rule of thumb for stability is not valid. In this scenario, the stable region is in fact smaller than predicted by usual theories (see **Fig. 7b.2**). Not taking this into account may be dangerous in real applications, since it could lead to unexpected instabilities.

Finally, let us investigate in more detail the conditions for the existence of a Hopf bifurcation, in the linear case ($\rho = 0$). As stated above, a Hopf bifurcation exists if

$$z = 1, \quad d_H < \eta < 0. \quad (59)$$

By substituting expressions (57) and (58) in (59), for $\rho = 0$, we have

$$z = 1, \quad -\frac{\alpha a_{eq} R_{eq}}{4\xi} < -\frac{\alpha a_{eq}^3 R_{eq}}{\xi} < 0. \quad (60)$$

Simplifying (60) yields

$$z = 1, \quad a_{eq} < 0.5. \quad (61)$$

Therefore, if the system under study has no structural nonlinearity ($\rho = 0$), it is particularly easy to predict the existence of a Hopf bifurcation, by simply checking condition (61).

5. Numerical Simulations

In this Section, some numerical experiments are performed in order to validate the analytical developments of Sections 3 and 4.

We analyse a system with the following parameter values:

$$\xi = 1, \quad \alpha = 1, \quad \rho = 0. \quad (62)$$

Two different situations are considered, corresponding to two different motor characteristics, T_{m1} and T_{m2} . Both of them intersect the vibration torque curve at point p and at two more points, as shown in **Fig. 8**. Consequently, the system exhibits three fixed points for any of the considered motor characteristics. These two curves are given by

$$T_{m1} = c_1 + d_1\sigma, \quad T_{m2} = c_2 + d_2\sigma, \quad (63)$$

with

$$c_1 = 0.3825, \quad d_1 = -0.074 \quad (64)$$

$$c_2 = 0.1866, \quad d_2 = -0.034. \quad (65)$$

On the other hand, point p can be shown to correspond to

$$\begin{aligned} z = 1, \quad a_{eq}(p) = 0.2 \\ \beta_{eq}(p) = -2.9402, \quad \sigma_{eq}(p) = 4.899. \end{aligned} \quad (66)$$

Note that the system under consideration has no structural nonlinearity ($\rho = 0$). Thus, by comparing (66) with (61), it can be stated that the stability of point p will change through a Hopf bifurcation when the motor characteristic is made to rotate around p .

Let us calculate the value of d_H at p . By using equation (58) we obtain

$$d_H = -0.049. \quad (67)$$

Observe that d_1 and d_2 are smaller and greater than d_H , respectively, as clearly shown in **Fig. 8**. Thus, according to the stability diagram in **Fig. 7b.2**, we expect fixed point p to be stable for $T_m = T_{m1}$, and unstable for $T_m = T_{m2}$. In addition, based on the stability diagrams in **Fig. 6a** and **Fig. 7b**, we can state that points r_1 and r_2 are stable, while q_1 and q_2 are unstable.

We have numerically solved equations (37), using embedded Runge–Kutta formulae of orders 4 and 5, for a number of initial conditions. In order to represent the phase plane, we consider a and β as polar coordinates, by defining

$$\begin{cases} x \equiv a \cos \beta \\ y \equiv a \sin \beta \end{cases} \quad (68)$$

The resulting phase portraits are shown in **Fig. 9**.

We find that r_1 and r_2 are stable nodes, q_1 and q_2 are saddle points and p is a stable (unstable) focus for $T_m = T_{m1}$ ($T_m = T_{m2}$). Thus, numerical results confirm the stability properties that had been analytically deduced.

Now, we conduct some additional numerical experiments in order to compare the solutions of the reduced system (37) to those of the original system (8). Three different simulations –**S1**, **S2** and **S3**– are carried out. Table 1 displays the initial conditions for system (8) at each simulation, as well as the chosen motor characteristic. The initial conditions for system (37), at each simulation, are computed according to (38).

Table 1
Initial Conditions and Motor Characteristic for each Simulation

S1	S2	S3
$T_m = T_{m1}$	$T_m = T_{m1}$	$T_m = T_{m2}$
$u_0 = 0.1$	$u_0 = 0.5$	$u_0 = 0.22$
$\dot{u}_0 = 0$	$\dot{u}_0 = 0$	$\dot{u}_0 = 0$
$\phi_0 = 0$	$\phi_0 = 0$	$\phi_0 = 3$
$\dot{\phi}_0 = 0$	$\dot{\phi}_0 = 0.5$	$\dot{\phi}_0 = 1$

Fig. 10-12 show the results for the three cases. They exhibit a remarkably good accordance between the solutions of both systems (original and reduced).

On the other hand, the coexistence of two stable equilibria for $T_m = T_{m1}$ is demonstrated in **Fig. 10** and **Fig. 11**. Depending on the initial conditions, the system evolves towards point p (**S1**) or point r_1 (**S2**).

Case **S3** is particularly interesting, for it shows that the Hopf bifurcation found in the reduced system occurs in the original one too. If relations (38) are applied to compute the initial conditions for the reduced system in case **S3**, we obtain

$$a_0 = 0.22, \quad \beta_0^* = -3. \quad (69)$$

This point is quite close to equilibrium p –see (66)–, and, consequently, it can be used to check whether p attracts or repels nearby trajectories. We already knew, from **Fig. 9**, that p is an unstable focus of the reduced system, for $T_m = T_{m2}$. **Fig. 12** further shows this is also true for the original system. Thus, we have been able to prove analytically the existence of a Hopf bifurcation, and also to demonstrate it by numerically solving the original equations of motion.

6. Discussion

6.1. Time Validity

A crucial point in any perturbation analysis is the time scale for which the obtained approximate solution is valid. It has been shown in Section 3 that the solution given by the reduced system is valid, at least, for a time scale $\tau = O(1/\epsilon)$ –see **Fig. 2**–.

However, the situation is even better than that. From the Averaging Theory, it is known [15] that a solution of the averaged system which tends to an asymptotically stable fixed point is valid for all $0 \leq \tau < \infty$. Note that this is the case for all the numerical solutions obtained in the last section.

6.2. Comparison with other authors' results

In this subsection, the presented approach and results are compared to some proposed by other authors.

First of all, as far as the authors know, there has been no attempt in the literature to use the SPT for the analysis of nonideally excited systems. Thus, the analytical procedure addressed in this paper appears to be a novel approach to the problem.

On the other hand, we have addressed the possibility of a Hopf bifurcation on the right branch of the vibration torque curve (**Fig. 7b.2**). An important implication of this result is that the stability of the stationary solutions near resonance does not only depends on the comparison between the slopes of the two torque curves ($\eta \leq d$), as commonly stated in the literature [7,8,10,30]. Let us try to explain this divergence in the results.

Kononenko's book [8] is one of the most relevant references in the subject. He considered several linear and nonlinear systems excited by nonideal motors. By using the averaging method, he was able to find an analytical solution to the equations of motion.

Considering the rotor speed to be in the vicinity of resonance, he expanded it as

$$\dot{\phi} = 1 + \Delta, \quad \Delta = \epsilon\sigma. \quad (70)$$

Thus, he found equations of the following form

$$\begin{aligned} \dot{a} &= O(\epsilon) \\ \dot{\beta} &= -\epsilon\sigma + O(\epsilon) \\ \dot{\Delta} &= O(\epsilon) \\ \dot{\phi} &= 1 + \Delta, \end{aligned} \quad (71)$$

which is a system analogous to (25). From the form of these equations, he deduced that variables a , β and Δ evolve with rate $O(\epsilon)$. Then, he interpreted (71) as a 4D dynamical system, with three slow state variables (a , β and Δ) and one fast state variable ϕ . Finally, he applied an averaging procedure in order to make the evolution of the slow variables independent of ϕ , transforming the system into a 3D one.

From our point of view, the above procedure may not be accurate enough, for the following reason. If system (71) was a 4D autonomous dynamical system, with state variables $\{a, \beta, \Delta, \phi\}$, then the r.h.s. of (71) would depend only on $\{a, \beta, \Delta, \phi\}$. Note, however, that also variable σ appears in the r.h.s. of (71). Therefore, a differential equation describing the evolution of variable σ needs to be added to the system:

$$\begin{aligned} \dot{a} &= O(\epsilon) \\ \dot{\beta} &= -\epsilon\sigma + O(\epsilon) \\ \dot{\Delta} &= O(\epsilon) \\ \dot{\sigma} &= O(1) \\ \dot{\phi} &= 1 + \Delta. \end{aligned} \quad (72)$$

System (72) underscores the presence of two fast variables in the system $-\sigma$ and $\dot{\phi}$, of which Kononenko only considered one. This is probably the reason of the difference between his results and ours.

While several authors followed Kononenko's approach [7,30], Blekhman proposed a completely different one, based on the 'method of direct separation of motions' [10]. With this procedure, he came to the conclusion that the system dynamics is governed by equation

$$I\ddot{\phi} = L(\dot{\phi}) + V(\phi) \quad (73)$$

where dimensional variables have been used. In (73), $V(\phi)$ represents the torque on the rotor due to vibration. Based on this equation, Blekhman deduced the same result as Kononenko regarding the stability of stationary

solutions, namely, that stability changes when the driving torque curve and the vibration torque curve are tangent.

We also find that Blekhman's approach may not be accurate enough. The reason is that, in general, the torque on the rotor due to vibration depends on the horizontal motion of the system, namely on variables a, β , as shown in the last of equations (28). This torque may only be written as a function of the rotor speed, $V(\dot{\phi})$, once a and β are particularized for a stationary solution of the system. This means that, using (73) to assess the stability of solutions implies neglecting the dynamics associated to variables a and β .

More recently, Bolla et al. [12] used the Multiple Scales method to solve the same problem studied in this paper, under the same assumptions. However, after obtaining system (28), they conducted the stability analysis considering only the first two equations in (28) and taking σ as a fixed parameter. As explained at the beginning of Section 4, this corresponds to studying the ideal case, where the rotor speed is externally imposed. Consequently, they did not find the Hopf bifurcations that have been identified within this work. In fact, Bolla et al. explicitly stated the impossibility of Hopf bifurcations: '*This fact eliminates the possibility of a pair eigenvalue pure imaginary, so this eliminates Hopf bifurcation kind*'. Thus, the present article can be envisaged as an extension of [12], where new bifurcations are encountered due to the nonideal interaction between motor and vibrating system.

7. Conclusions

The present paper is concerned with the analytical and numerical analysis of a nonlinear vibrating system, excited by an unbalanced motor. The main contributions of this work are summarized as follows:

- A novel analytical approach to the problem, which combines an averaging procedure with the SPT, has been proposed. It is worth stressing that, although both the SPT and the Averaging Method are actually classical in nonlinear dynamics, they had not been used together before in the context of nonideal excitations. Thanks to this novel combination of perturbation techniques, the original 4D system is asymptotically approximated by a reduced 2D system, which is much easier to analyse.
- The conditions for stability of equilibria of the reduced system have been analytically derived. Transcritical and Hopf bifurcations have been found. The Hopf bifurcation is particularly relevant, for it gives rise to a smaller stable region than predicted by conventional theories. Consequently, not taking it into account may be perilous for real applications, since unexpected instabilities could occur.
- The analytical developments presented here have been validated by comparing numerical solutions of the original and reduced systems. In particular, the Hopf bifurcation existence has been numerically proved, not only for the reduced system, but, more importantly, also for the original system of equations.

Acknowledgements This work was supported by Grant FPU12/00537 of the Spanish Ministry of Education, Culture and Sport. The authors gratefully acknowledge the help of Prof. Emilio Freire with the applied mathematical techniques.

References

- [1] A. Boyaci, D. Lu, B. Schweizer, Stability and bifurcation phenomena of Laval/Jeffcott rotors in semi-floating ring bearings, *Nonlinear Dynamics*. 79 (2015) 1535–1561. doi:10.1007/s11071-014-1759-5.
- [2] J. Yang, Y. Gao, Z. Liu, C. Zhao, T. Kang, L. Gu, B. Xu, A method for modeling and analyzing the rotor dynamics of a locomotive turbocharger, *Nonlinear Dynamics*. 84 (2016) 287–293. doi:10.1007/s11071-015-2497-z.
- [3] A.A. Shabana, *Theory of vibration (An Introduction)*, 1996. doi:10.1016/0378-3804(84)90129-3.
- [4] M. Xu, R.D. Marangoni, Vibration Analysis of a Motor-Flexible Coupling-Rotor System subject to Misalignment and Unbalance, Part I: Theoretical Model and Analysis, *Journal of Sound and Vibration*. 176 (1994) 663–679.
- [5] W.T. Thomson, *Theory of Vibration with Applications*, 1996. doi:10.1121/1.1901874.
- [6] A. Sommerfeld, *Naturwissenschaftliche Ergebnisse der Neuren Technischen Mechanik*, Verein Dtsch. Ing. Zeitschrift. 18 (1904) 631–636. doi:10.1109/COC.2000.873973.
- [7] A.H. Nayfeh, D.T. Mook, *Nonlinear Oscillations*, John Wiley and Sons, 1995.
- [8] V.O. Kononenko, *Vibrating Systems with a limited power supply*, Illife, London, 1969.
- [9] R.H. Rand, R.J. Kinsey., D.L. Mingori, Dynamics of spinup through resonance, *International Journal of Non-Linear Mechanics*. 27 (1992) 489–502. doi:10.1016/0020-7462(92)90015-Y.
- [10] I.I. Blekhman, *Vibrational Mechanics-Nonlinear Dynamic Effects, General Approach*, Singapore, 2000.
- [11] A.A. El-Badawy, Behavioral Investigation of a Nonlinear Nonideal Vibrating System, *Journal of Vibration and Control*. 13 (2007) 203–217. doi:10.1177/1077546307073674.
- [12] D.T. Bolla, M. R., Balthazar, J. M., Felix, J. L. P., Mook, On an approximate analytical solution to a nonlinear vibrating problem , excited by a nonideal motor, *Nonlinear Dynamics*. (2007) 841–847. doi:10.1007/s11071-007-9232-3.
- [13] M.J.H. Dantas, J.M. Balthazar, J.L.P. Félix, On the Appearance of Neimark-Sacker Bifurcation in a Non-Ideal System, in: *Int. Conf. Vib. Probl.*, Lisboa, 2013.
- [14] J.M. Balthazar, D.T. Mook, H.I. Weber, B. R., A. Fenili, D. Belato, J.L.P. Felix, An Overview on Non-Ideal Vibrations, *Meccanica*. 38 (2003) 613–621.
- [15] J.A. Sanders, F. Verhulst, J. Murdock, *Averaging Methods in Nonlinear Dynamical Systems*, Springer, New York, 2007.
- [16] A. Lesne, *Multi-scale Approaches*, Lab. Phys. La Matière Condens. Univ. Pierre Marie Curie. (2006).
- [17] F. Verhulst, T. Bakri, The Dynamics of Slow Manifolds, *Journal of the Indonesian Mathematical Society*. (2006) 1–16.
- [18] J.K. Hunter, *Asymptotic Analysis and Singular Perturbation Theory*, Department of Mathematics, University of California at Davis. (2004).
- [19] Y.A. Kuznetsov, *Elements of Applied Bifurcation Theory*, Second Edition, New York, 1998.
- [20] J. Guckenheimer, P. Holmes, *Nonlinear Oscillations, Dynamical Systems, and Bifurcations of Vector Fields*, Springer New York, New York, NY, 1983. doi:10.1007/978-1-4612-1140-2.
- [21] M.J.H. Dantas, J.M. Balthazar, On the appearance of a Hopf bifurcation in a non-ideal mechanical problem, *Mechanics Research Communications*. 30 (2003) 493–503. doi:10.1016/S0093-6413(03)00041-7.
- [22] J.L.P. Felix, J.M. Balthazar, Comments on a nonlinear and nonideal electromechanical damping vibration absorber, Sommerfeld effect and energy transfer, *Nonlinear Dynamics*. 55 (2009) 1–11. doi:10.1007/s11071-008-9340-8.
- [23] J.L.P. Felix, J.M. Balthazar, M.J.H. Dantas, On energy pumping, synchronization and beat phenomenon in a nonideal structure coupled to an essentially nonlinear oscillator, *Nonlinear Dynamics*. 56 (2009) 1–11. doi:10.1007/s11071-008-9374-y.

- [24] T.S. Krasnopolskaya, A.Y. Shvets, Chaos in vibrating systems with a limited power-supply., *Chaos*. 3 (1993) 387–395. doi:10.1063/1.165946.
- [25] A. Fidlin, *Nonlinear Oscillations in Mechanical Engineering*, Springer–Verlag, Berlin, Heidelberg, 2006.
- [26] D. Quinn, R. Rand, J. Bridge, The dynamics of resonant capture, *Nonlinear Dynamics*. 8 (1995) 1–20. doi:10.1007/BF00045004.
- [27] D. Belato, H.I. Weber, J.M. Balthazar, D.T. Mook, Chaotic vibrations of a nonideal electro-mechanical system, *International Journal of Solids and Structures*. 38 (2001) 1699–1706. doi:10.1016/S0020-7683(00)00130-X.
- [28] M. Zukovic, L. Cveticanin, Chaos in Non-ideal Mechanical System with Clearance, *Journal of Vibration and Control*. 15 (2009) 1229–1246. doi:10.1177/1077546308091216.
- [29] E. Mettler, *Handbook of Engineering Mechanics*, McGraw-Hill, New York, 1962.
- [30] M.F. Dimentberg, L. Mcgovern, R.L. Norton, J. Chapdelaine, R. Harrison, Dynamics of an Unbalanced Shaft Interacting with a Limited Power Supply, *Nonlinear Dynamics*. (1997) 171–187. doi:10.1023/a:1008205012232.
- [31] L. Cveticanin, M. Zukovic, Motion of a motor-structure non-ideal system, *European Journal of Mechanics - A/Solids*. 53 (2015) 229–240. doi:10.1016/j.euromechsol.2015.05.003.
- [32] W. Eckhaus, *Asymptotic Analysis of Singular Perturbations*, North- Holland Publ. Co., Amsterdam, 1979.
- [33] J.J. Thomsen, *Vibrations and Stability*, Berlin, Heidelberg, New York, 2003.
- [34] M.J. Brennan, I. Kovacic, A. Carrella, T.P. Waters, On the jump-up and jump-down frequencies of the Duffing oscillator, *Journal of Sound and Vibration*. 318 (2008) 1250–1261. doi:10.1016/j.jsv.2008.04.032.
- [35] I. Kovacic, M.J. Brennan, B. Lineton, On the resonance response of an asymmetric Duffing oscillator, *International Journal of Non-Linear Mechanics*. 43 (2008) 858–867. doi:10.1016/j.ijnonlinmec.2008.05.008.
- [36] J. Holtz, I. Paper, J. Holtz, Sensorless control of induction motor drives, *Proc. IEEE*. 90 (2002) 1359–1394. doi:10.1109/JPROC.2002.800726.

Appendix: Derivation of the Averaged System

The transformation of system (25) into (28) is justified below.

System (25) has the form

$$\begin{aligned}
 \dot{a} &= -\epsilon f(a, \beta, \phi) + O(\epsilon^2) \\
 \dot{\beta} &= -\epsilon \sigma - \epsilon g(a, \beta, \phi) + O(\epsilon^2) \\
 \dot{\sigma} &= d\sigma + h(a, \beta, \phi) + O(\epsilon) \\
 \dot{\phi} &= 1 + O(\epsilon),
 \end{aligned} \tag{A1}$$

where functions f , g and h are 2π -periodic in ϕ .

We would like to apply the averaging method to system (A1), in order to eliminate the angular variable ϕ and obtain a simpler 3D system. In general, for the method to be applicable, we would need variables a , β and σ to be slow. Since we observe that σ is a fast variable, it may be thought that the averaging procedure cannot be applied in this case.

Fortunately, system (A1) has the particularity that fast variable σ only appears linearly on the r.h.s. of the equations. We will show that this feature allows for an averaging procedure.

Averaging system (A1) yields

$$\begin{aligned}\dot{\bar{a}} &= -\epsilon \bar{f} + O(\epsilon^2) \\ \dot{\bar{\beta}} &= -\epsilon \bar{\sigma} - \epsilon \bar{g} + O(\epsilon^2) \\ \dot{\bar{\sigma}} &= d\bar{\sigma} + \bar{h} + O(\epsilon),\end{aligned}\tag{A2}$$

where we have used the fact that the average, defined in (27), is a linear operator. The remaining task consists in finding the averaged functions \bar{f} , \bar{g} and \bar{h} . Since the calculation is analogous for the three of them, we will focus on \bar{f} . Applying definition (27), we have

$$\bar{f}(\tau) \equiv \frac{1}{2\pi} \int_{\tau-\pi}^{\tau+\pi} f(a(s), \beta(s), \phi(s)) ds.\tag{A3}$$

By using relations (29), we write (A3) as

$$\bar{f}(\tau) = \frac{1}{2\pi} \int_{\tau-\pi}^{\tau+\pi} f(\bar{a}(\tau), \bar{\beta}(\tau), \phi(s)) ds + O(\epsilon).\tag{A4}$$

Let us now change the integration variable:

$$\bar{f}(\tau) = \frac{1}{2\pi} \int_{\phi(\tau-\pi)}^{\phi(\tau+\pi)} f(\bar{a}(\tau), \bar{\beta}(\tau), \phi) d\phi + O(\epsilon),\tag{A5}$$

where we have used $\dot{\phi} = 1 + O(\epsilon)$. This can be rewritten as

$$\bar{f}(\tau) = \frac{1}{2\pi} \int_{\phi(\tau)-\pi}^{\phi(\tau)+\pi} f(\bar{a}(\tau), \bar{\beta}(\tau), \phi) d\phi + O(\epsilon).\tag{A6}$$

Using the property that f is 2π -periodic in ϕ , we have

$$\bar{f}(\tau) = \frac{1}{2\pi} \int_0^{2\pi} f(\bar{a}(\tau), \bar{\beta}(\tau), \phi) d\phi + O(\epsilon).\tag{A7}$$

By simply applying expression (A7) to functions f , g and h , we arrive at

$$\begin{aligned}
 \bar{f}(\tau) &= \xi(\bar{a}(\tau) + \sin[\bar{\beta}(\tau)]) + O(\epsilon) \\
 \bar{g}(\tau) &= \xi \frac{\cos[\bar{\beta}(\tau)]}{\bar{a}(\tau)} - \frac{3}{8}\rho\bar{a}^2(\tau) + O(\epsilon) \\
 \bar{h}(\tau) &= c + \frac{\alpha}{2}\bar{a}(\tau) \sin[\bar{\beta}(\tau)] + O(\epsilon).
 \end{aligned}
 \tag{A8}$$

Finally, introducing (A8) into (A2) yields the averaged system (28).

Figures

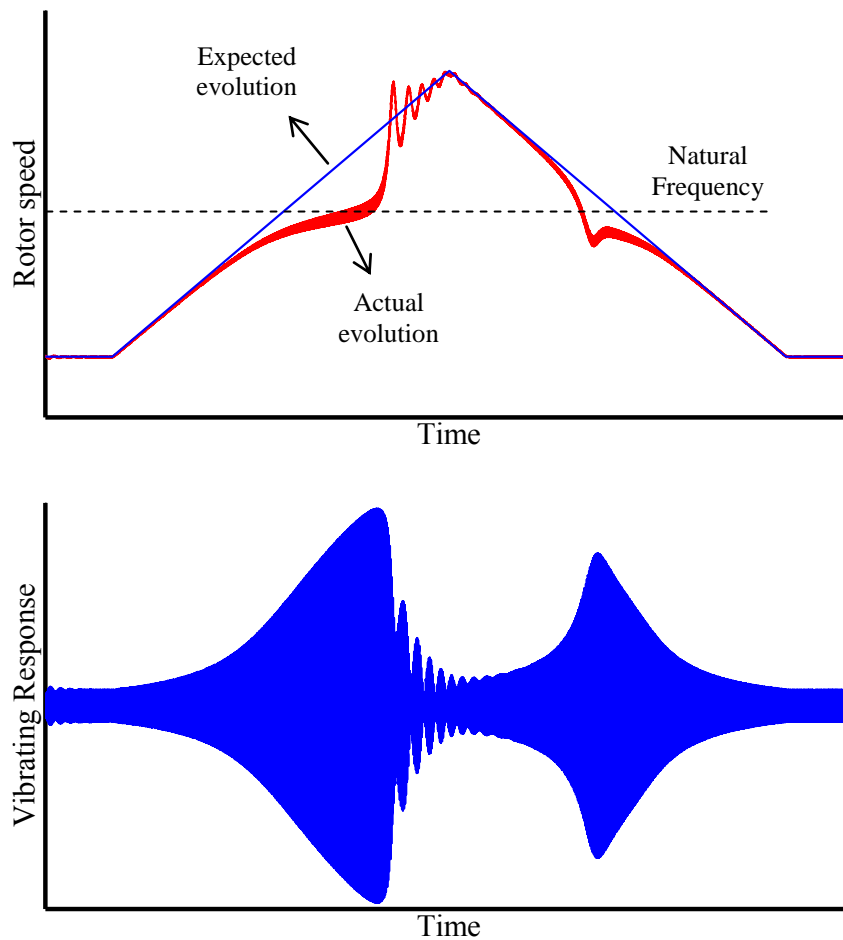


Fig. 1 Sommerfeld Effect

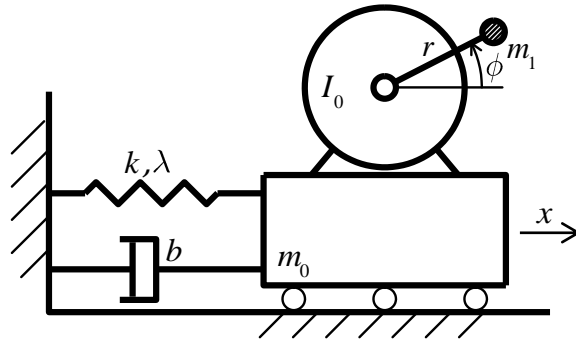


Fig. 2 Model

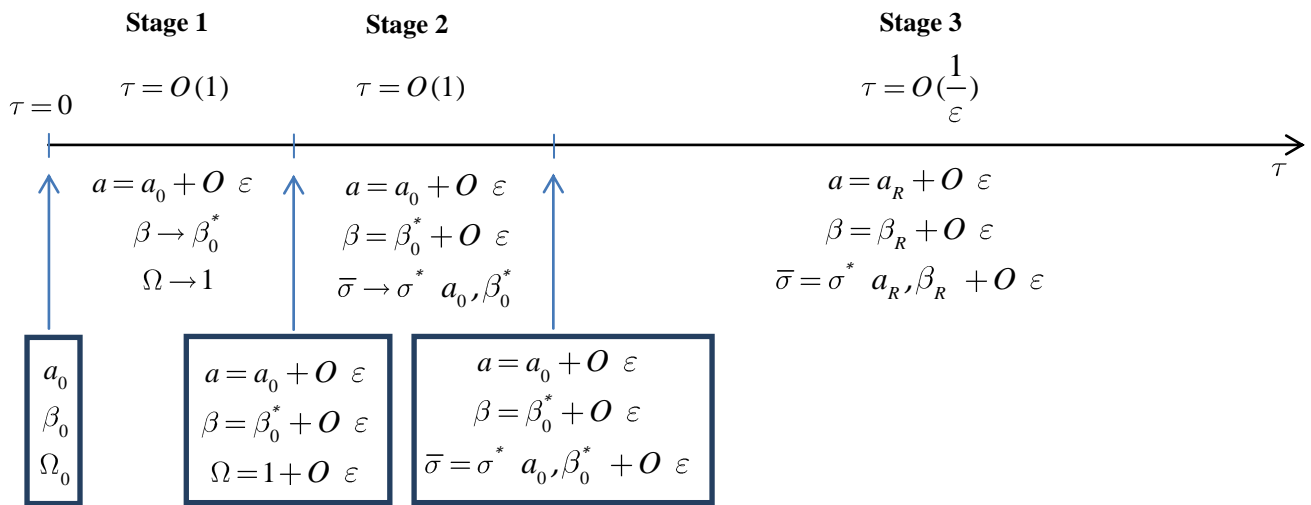


Fig. 3 Overview of the system dynamics.

a_R and β_R solution of system (37), with appropriate initial conditions

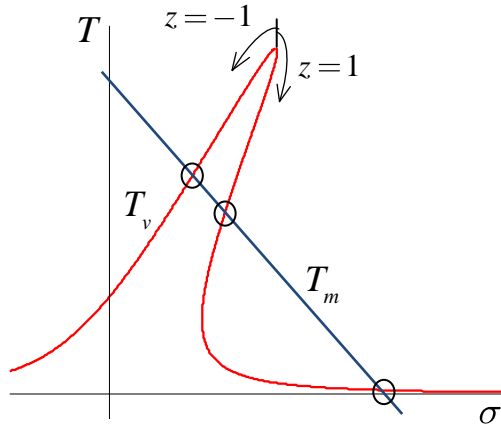


Fig. 4 Fixed points of (37)

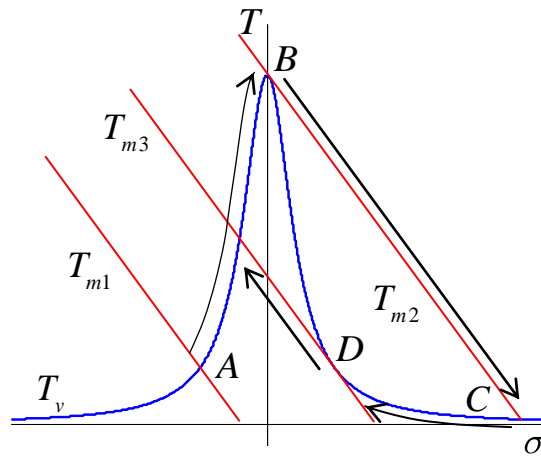


Fig. 5 Explanation of the Sommerfeld Effect

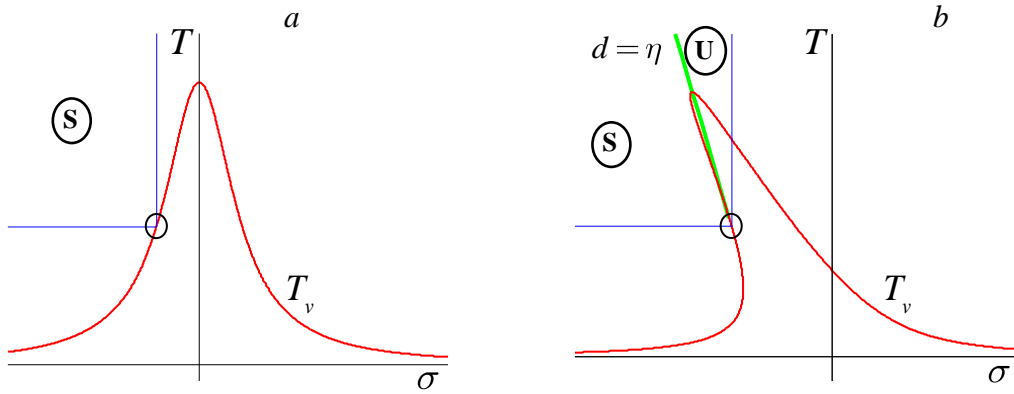


Fig. 6 Stability regions for $z = -1$. S and U label the stable and unstable regions, respectively.

(a) $\eta > 0$

(b) $\eta < 0$

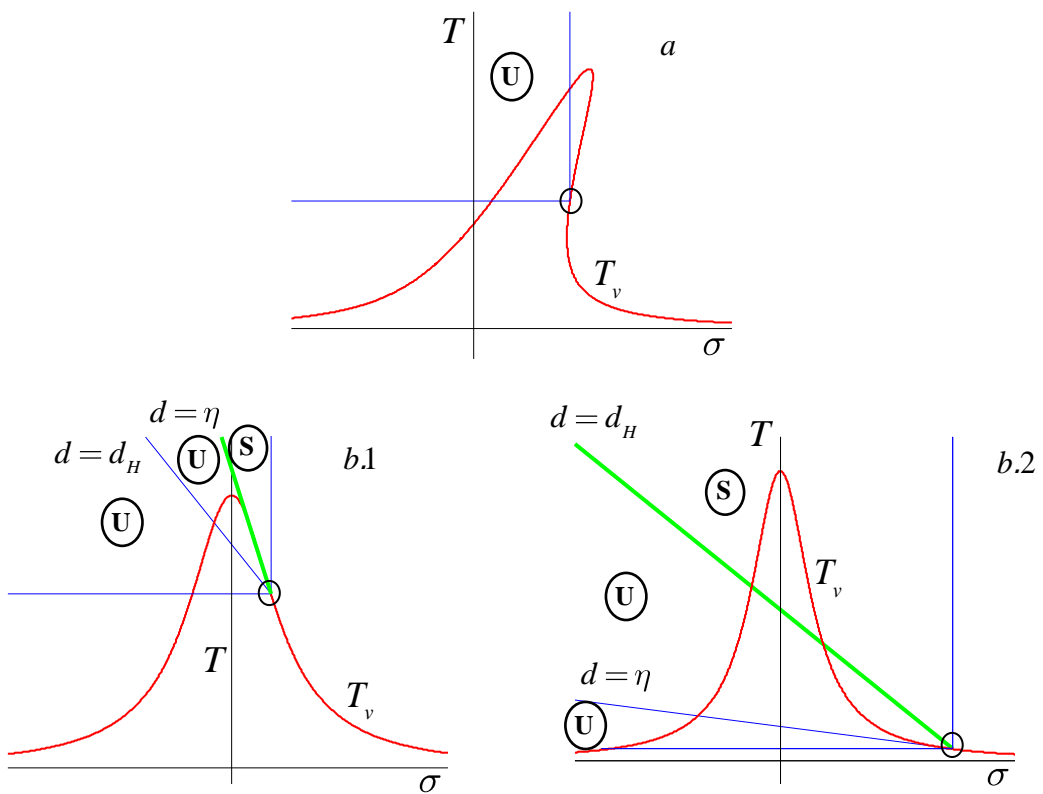


Fig. 7 Stability regions for $z = 1$. S and U label the stable and unstable regions, respectively.

(a) $\eta > 0$

(b.1) $\eta < d_H < 0$

(b.2) $d_H < \eta < 0$

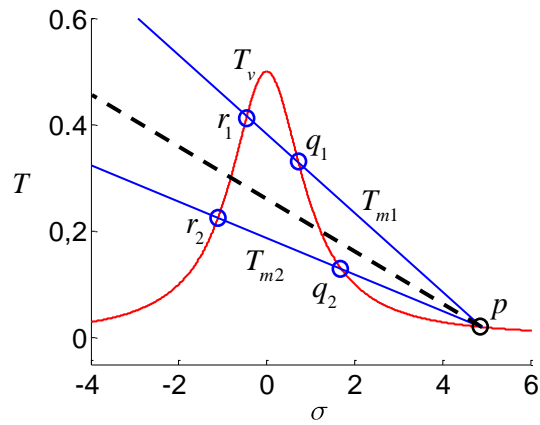


Fig. 8 Torque curves

The dashed straight line corresponds to the bifurcation point $d = d_H$

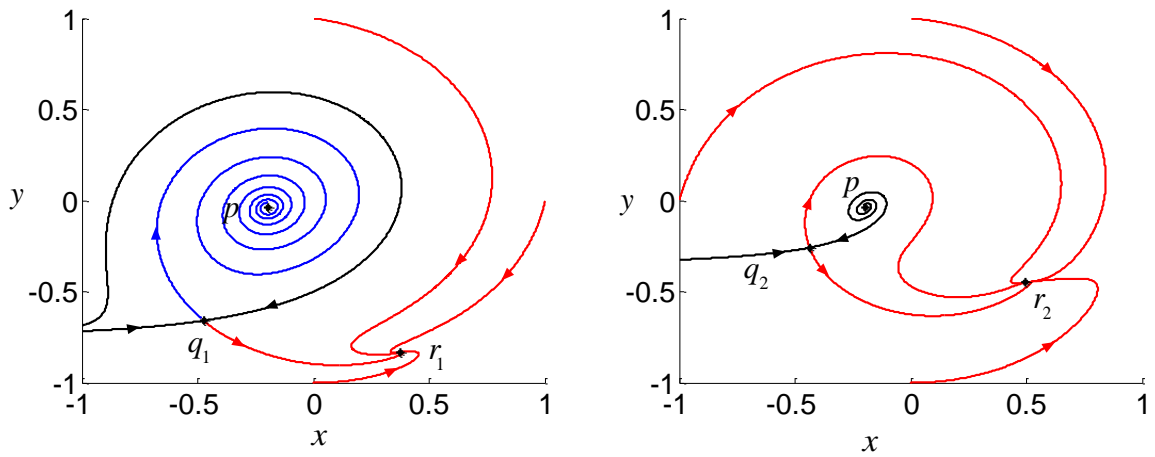


Fig. 9 Phase portrait for

(a) $T_m = T_{m1}$

(b) $T_m = T_{m2}$

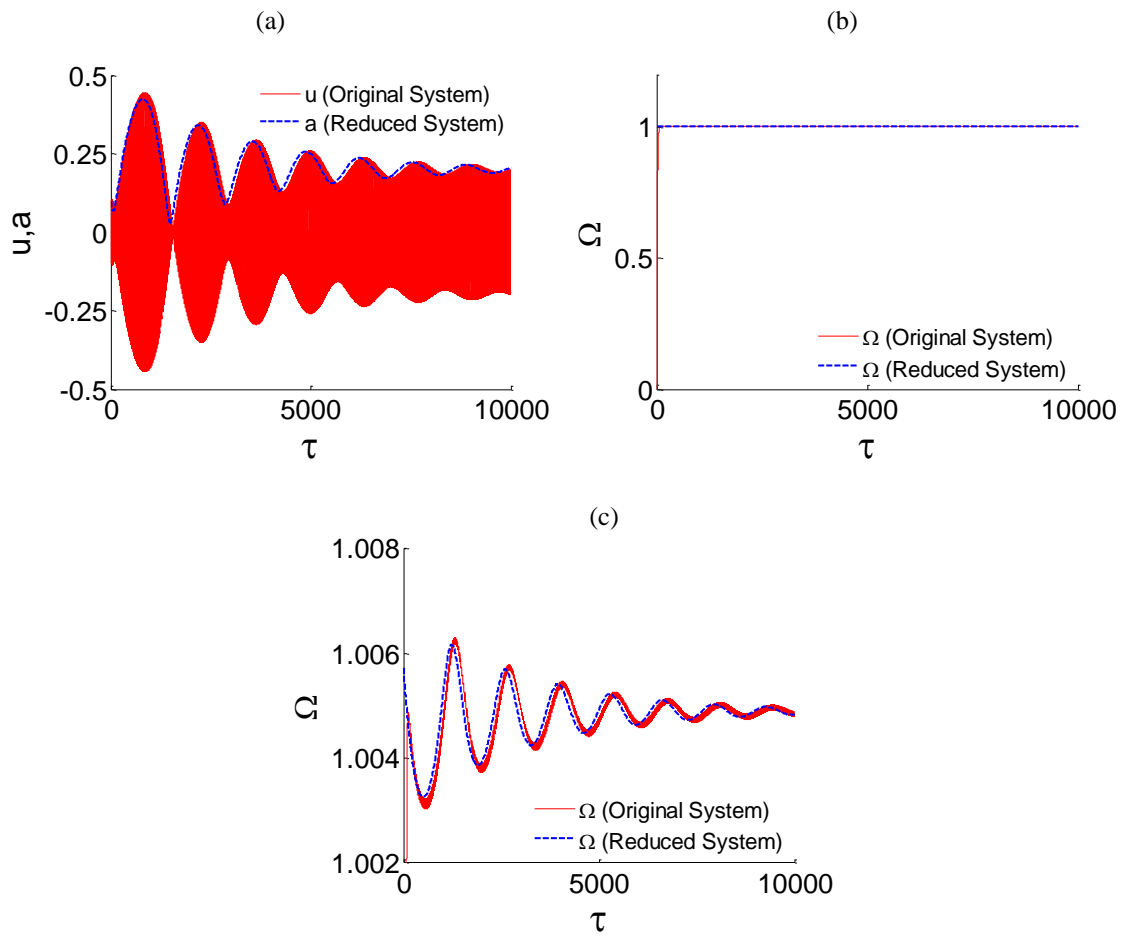


Fig. 10 Results of Simulation S1 with $\epsilon = 10^{-3}$

(a) Displacement

(b) Rotor Speed (Full view)

(c) Rotor Speed (Close-up around resonance)

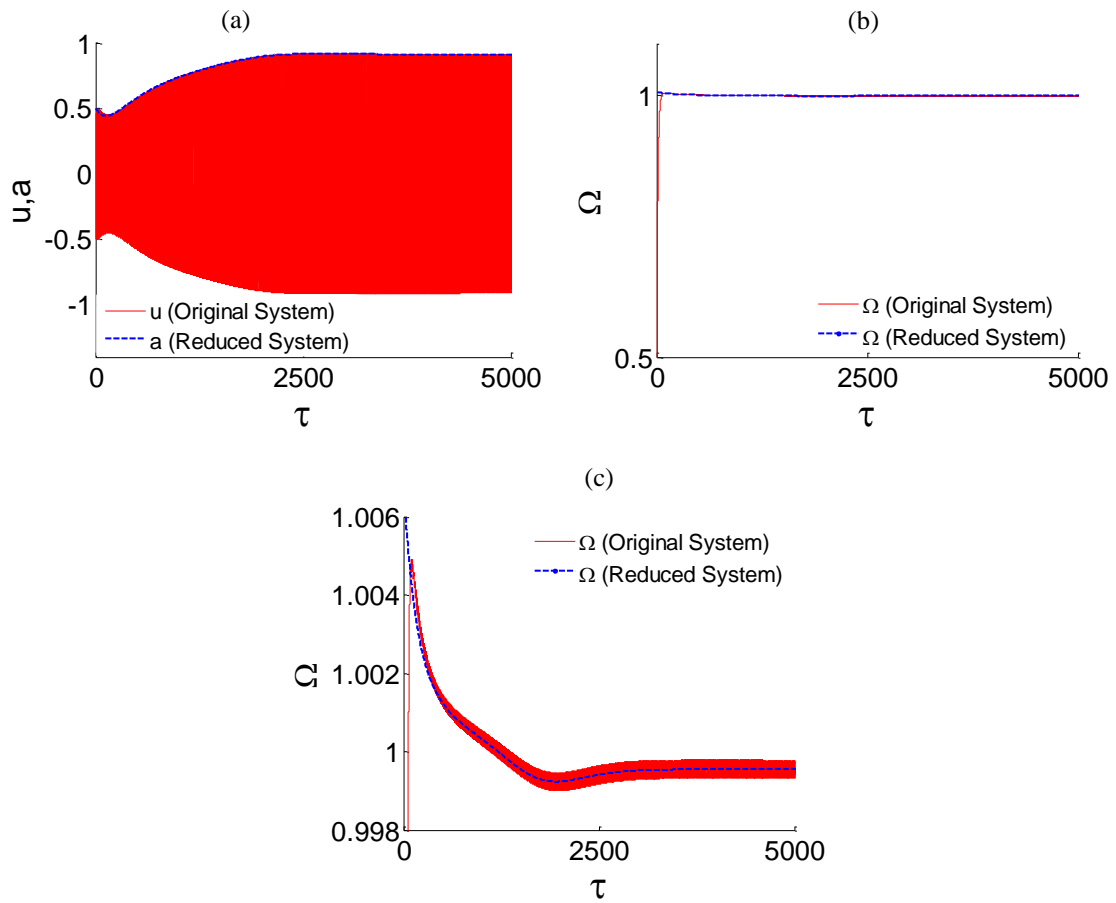


Fig. 11 Results of Simulation S2 with $\epsilon = 10^{-3}$

(a) Displacement

(b) Rotor Speed (Full view)

(c) Rotor Speed (Close-up around resonance)

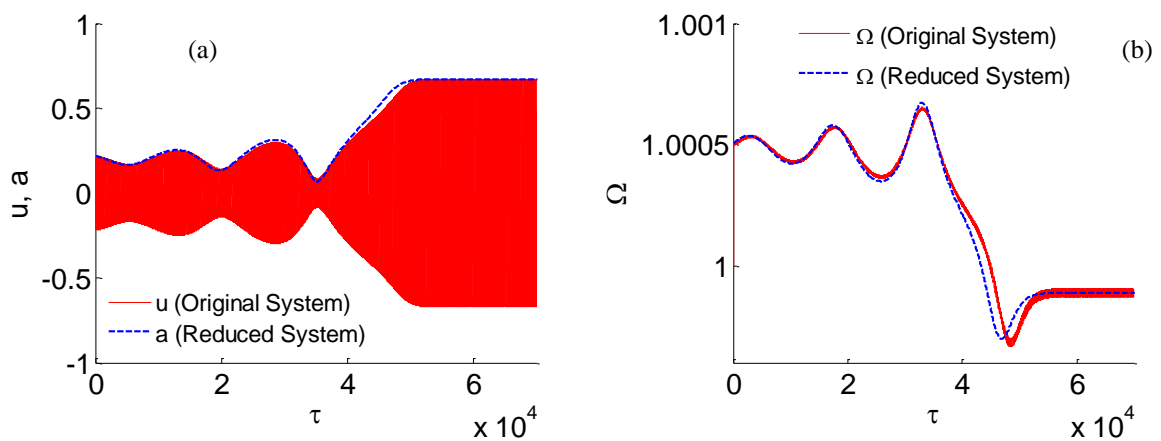


Fig. 12 Results of Simulation S3 with $\epsilon = 10^{-4}$

(a) Displacement

(b) Rotor Speed